

Gas-phase infrared spectra of cationized nitrogen-substituted polycyclic aromatic hydrocarbons

H. Alvaro Galué¹, O. Pirali², and J. Oomens^{1,3}

¹ FOM Institute for Plasma Physics “Rijnhuizen”, Edisonbaan 14, 3439MN Nieuwegein, The Netherlands
e-mail: H.AlvaroGalue@rijnhuizen.nl

² Synchrotron SOLEIL, L’Orme des Merisiers Saint-Aubin, 91192 Gif-sur-Yvette Cedex, France
e-mail: olivier.pirali@synchrotron-soleil.fr

³ Van ’t Hoff Institute for Molecular Sciences, University of Amsterdam, Nieuwe Achtergracht 166, 1018 WV Amsterdam, The Netherlands
e-mail: joso@rijnhuizen.nl

Received 12 January 2010 / Accepted 30 March 2010

ABSTRACT

Gas-phase infrared spectra of several ionized nitrogen substituted polycyclic aromatic hydrocarbons (PANHs) have been recorded in the 600–1600 cm⁻¹ region via IR multiple-photon dissociation (IRMPD) spectroscopy. The UV photoionized PANH ions are trapped and isolated in a quadrupole ion trap where they are irradiated with an IR free electron laser. The PANHs were studied in their radical cation (PANH⁺) and protonated (H⁺PANH) forms, and include quinoline, isoquinoline, phenanthridine, benzo[h]quinoline, acridine, and dibenzof[h]quinoline. Experimental IRMPD spectra were interpreted with the aid of density functional theory methods. The PANH⁺ IR spectra are found to resemble those of their respective non-nitrogenated PAH cations. The IR spectra of H⁺PANHs are significantly different owing to the NH inplane bending vibration, which generally couples very well with the aromatic CH bending and CC stretching modes. Implications of the NPAH (+, H⁺) laboratory spectra are discussed for the astrophysical IR emissions and, in particular, for the band at 6.2 μm.

Key words. astrochemistry – methods: laboratory – techniques: spectroscopic – ISM: molecules – molecular processes

1. Introduction

The infrared (IR) emission features commonly referred to as the unidentified infrared bands (UIRs) observed in most major classes of astrophysical sources at 3.3, 6.2, 7.7, 8.6, 11.3 μm (Leger & Puget 1984) are recognized as being carried by a broad molecular family of polycyclic aromatic hydrocarbons (PAHs). The actual appearance of the UIR spectrum is strongly affected by the physics and chemistry prevailing within the source (Joblin 1998; Tielens 2008; Hony et al. 2001; Peeters et al. 2002). Understanding these variations and how they induce changes in relative intensities, peak positions, and profiles is linked with the general idea of rationalizing how the environment sustains and modifies the physical properties of the PAH family (size, structure, ionization state, dehydrogenation, protonation, etc.).

Laboratory IR spectroscopy, including gas-phase, solid state, and matrix-isolation techniques, has been useful in probing the IR activity of vibrational modes of bare PAHs in neutral (Hudgins & Allamandola 1999a; Joblin et al. 1994; Pirali et al. 2006) and ionic forms (Hudgins & Allamandola 2002; Kim et al. 2001; Oomens et al. 2001, 2003, 2000; Piest et al. 1999; Szczepanski & Vala 1993a,b), which generally reproduce the features of the UIR emissions (Allamandola et al. 1999; Bregman et al. 2000; Sloan et al. 1999; Tielens 2008). Nonetheless, the identification of a specific PAH species or even of a subfamily as the main contributor to a spectral variation of a particular band has not been established experimentally.

The UIR emissions, and how these are attributed to PAH molecules and ions, has been the subject of a recent review (Tielens 2008). Briefly, the 6.2 (1612 cm⁻¹) and 7.7 μm

(1298 cm⁻¹) emissions involve the CC stretching vibrations, and the 8.6 μm (1162 cm⁻¹) and longer wavelength emissions involve the CH bending “inplane” and “out-of-plane” vibrations. The 3.3 μm (3030 cm⁻¹) band is attributed to CH stretching modes. Special interest has been focused on the 6.2 μm band because the interstellar emission generally appears at higher frequencies than those reproduced by PAH cations in laboratory spectroscopic studies. Various PAH modifications have therefore been proposed to induce this sensitive spectral shift, for instance, larger PAH sizes, N-substituted PAH cations, closed-shell cationic PAHs, and aliphatic groups (Beegle et al. 2001; Hudgins & Allamandola 1999b; Hudgins et al. 2001, 2005; Peeters et al. 2002; Pino et al. 2008).

The hypothesis of nitrogen containing PAHs occurring in interstellar environments has been considered extensively (Bernstein et al. 2005; Charnley et al. 2005; Elsila et al. 2006; Hudgins et al. 2005; Mattioda et al. 2003, 2008; McNaughton et al. 2008; Peeters et al. 2002, 2005; Mattioda et al. 2005; Ricca et al. 2001; Tielens 2008) since nitrogen is one of the most abundant elements after hydrogen, helium, and carbon. These species are known as polycyclic aromatic nitrogen heterocycles (PANHs). They have been identified in carbonaceous chondrite meteorites (Sephton 2002) and are expected to form in the interstellar medium (ISM) if nitrogen-bearing molecules are present (Ricca et al. 2001). The formation and photostability of small PANHs was previously discussed with the conclusion that only an astrophysical environment typical of a dense molecular cloud can host these species (Peeters et al. 2005). Finally, because of their higher permanent dipole moment, PANHs are an interesting class of polyaromatics since they can be detected by

Table 1. PANH species studied in this work.

Name	Chemical formula	PANH ⁺ (<i>m/z</i>)	H ⁺ PANH (<i>m/z</i>)
Quinoline	C ₉ H ₇ N	129	130
Isoquinoline	C ₉ H ₇ N	129	130
Benzo[h]quinoline	C ₁₃ H ₉ N	179	...
Phenanthridine	C ₁₃ H ₉ N	179	180
Acridine	C ₁₃ H ₉ N	179	180
Dibenzo[f,h]quinoline	C ₁₇ H ₁₁ N	229	...

microwave spectroscopy more readily than unsubstituted PAHs (McNaughton et al. 2008; Don McNaughton & Thorwirth 2007). However, searches for PANH species in the ISM based on these pure rotational spectra have thus far been unsuccessful (Charnley et al. 2005).

Atomic nitrogen is iso-electronic with a CH group, hybridizes as 120° sp² orbitals, and forms one single and one double bond with two neighboring carbons, conserving the planarity of the aromatic molecule. The π -electron system is not compromised thus retaining its thermodynamic stability as required in astrophysical environments. Based on computations that studied the effect of N-atom substitution into the PAH carbon skeleton on the CC stretching-mode frequencies (Mattioda et al. 2003; Peeters et al. 2002), it was proposed that large PAHs with the N-atom substituted inside the aromatic network (endoskeletal) reproduce the 6.2 μ m band, due to the combined effect of heterogeneity and closed-shell electronic structure resulting from the endoskeletal N substitution (Hudgins et al. 2005). PANHs in which N for C substitution occurs on the periphery (exoskeletal), thus having an open-shell structure in their cationic form, were not considered to be promising candidates because the CC stretching modes occur slightly redshifted. However, since endoskeletal N-substituted PAHs are not commercially available (due to their radical nature as a neutral molecule), this hypothesis has not been verified in the laboratory.

The nitrogen lone-pair electrons of a PANH are not delocalized in the π system, and a neutral PANH can readily donate its electrons to the 1s-orbital of ionized atomic hydrogen, forming a stable, closed-shell, protonated PANH ion. Indeed, because of the high proton affinity of these species, it is not unlikely that they occur in their protonated forms. Recent experiments involving ion spectroscopy of various protonated PAH species report absorption bands very close to the 6.2 μ m interstellar band (Douberly et al. 2008; Knorke et al. 2009; Lorenz et al. 2007; Ricks et al. 2009; Vala et al. 2009a,b), although a detailed comparison between all protonated PAH spectral features and the interstellar UIR bands has not been performed to date. These protonated PAHs also have a closed-shell electronic structure.

In this work we present an IR ion spectroscopy investigation of six ionized PAH structures with an N-atom substituted in one of the outer rings. The PANH molecules investigated in protonated (H⁺PANH) and radical (PANH⁺) forms are listed in Table 1. The fundamental difference between H⁺PANH and PANH⁺ is the closed versus open-shell electronic configuration, which may induce differences in bond strengths, resulting in distinctive infrared spectral characteristics for each of the ionic forms.

The spectroscopic method employed here is based on the resonant IR multiple photon dissociation (IRMPD) of PANH ions in the gas phase using a free electron laser described in the next section. In the subsequent section, the measured IRMPD spectra are described for the six PANH structures and differences

between H⁺PANH and PANH⁺ spectra for each structure are discussed. What follows is a discussion of the relevance of the PANH (+, H⁺) spectra to the UIR bands. It is found that protonated nitrogen containing PAHs may contribute to the UIR bands at 6.2 and 8.6 μ m.

2. Methods

2.1. Experimental

The experimental method used to obtain gas-phase infrared ion spectra is based on multiple-photon excitation of gas-phase PANH ions stored in a Paul-type quadrupole ion trap (Paul 1990) using the intense IR output of a free electron laser. This method has already been employed to investigate unsubstituted PAH cations, so a detailed description can be found elsewhere (Oomens et al. 2000). IR pulses are generated by the Free Electron Laser for Infrared eXperiments (FELIX) (Oepts et al. 1995). FELIX delivers 5- μ s long macropulses at a repetition rate of 5 or 10 Hz, each with up to 100 mJ of energy and composed of some 5000 micropulses around 1 ps long. The laser bandwidth is Fourier-transform limited by the micropulse duration and is typically 0.5% of the central wavelength in the present experiments. When the IR frequency of the radiation is in resonance with an allowed transition of the ionic species, many photons are absorbed, generating an internal energy distribution that (partly) exceeds the threshold for unimolecular dissociation (Bagratashvili et al. 1985). The intensity of photo-fragment ions, as well as the remaining parent ion, is recorded using a linear time-of-flight (TOF) mass spectrometer equipped with a multichannel plate (MCP) detector. The fragment ion yield as a function of IR wavelength yields the infrared multiple-photon dissociation (MPD) spectrum, which has been shown by many examples to be a good surrogate for the IR absorption spectrum (Oomens et al. 2003).

In the current experiments, the three electrodes of the quadrupole ion trap are biased at a positive voltage of typically 1385 V. The 2-cm inner diameter toroidal ring electrode in addition carries a 1 MHz radio frequency (RF) voltage. The stability of the three-dimensional ion trajectories is determined by the RF amplitude, which is set to values between 500 and 2000 V_{p-p} depending on the mass of the ionic species studied. Axial extraction of ions is done by applying a pulsed voltage dip (−200 V) to the endcap electrode nearest to the detector.

The liquid samples are placed in a pyrex tube and their vapor effuses to the center of the trap via a needle valve. For solid, low vapor-pressure samples, a graphite oven placed inside the vacuum chamber is used for evaporating the sample. To ionize the molecules, an ArF excimer laser (193 nm) is focused at the center of the trap, where parent ion and possible UV-induced fragment ions are instantaneously trapped. The fragments are axially ejected by momentarily (2 ms) increasing the RF amplitude. The ionization potentials of the investigated PANHs fall in the 8–9 eV range (Dewar & Worley 1969), and the non-resonant absorption of two 193-nm photons (12.8 eV) will remove one of the electrons in the highest occupied molecular orbital (HOMO), which is located at the aromatic π -system (Dewar & Worley 1969; Dolgounitcheva et al. 1997). Any excitation in the electronic levels of the ion is expected to be rapidly relaxed to the doublet ground state of the ion via internal conversion, possibly producing ions with some degree of vibrational excitation (Lifshitz 1983). After ionization, the ions are trapped for 3 ms in order to promote a uniform distribution of translational energies of the ions (Baer & Hase 1996; Oomens et al. 2002). Thereafter,

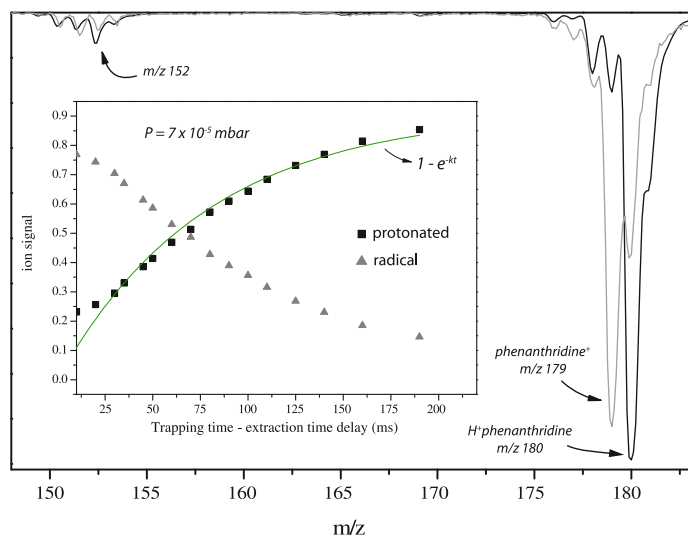


Fig. 1. Mass spectra of phenanthridine showing the radical, protonated, and IRMPD-induced fragment ionic signals. The inset shows the change of phenanthridine⁺ and H⁺phenanthridine intensities as a function of trapping time at a fixed pressure. The formation of H⁺phenanthridine is governed by first-order kinetics as indicated by the fit to a $1 - \exp(-kt)$ function.

they are subject to interaction with a high-fluence IR pulse inducing multiple photon dissociation (MPD).

When FELIX is tuned in resonance with a vibrational mode of the ion, a photon is absorbed, and the energy is rapidly diffused via intramolecular vibrational redistribution (IVR) over the bath of vibrational background states of the ion (Lehmann et al. 1994). The IVR lifetimes at room temperature of PAHs are less than 1 ns (Felker & Zewail 1985), and assuming that these lifetimes are similar for N-substituted PAHs, the population of PANH ions in the excited bright state is removed by IVR so that these ions are ready for interaction with the next FELIX micropulse. The IRMPD induced fragments and parent ion are mass-analyzed with the TOF mass spectrometer, and the dissociation ion yield is computed as $I_{fi}/I_{fi} + I_p$; where I_{fi} and I_p are the integrated intensities of the i th fragment and of the parent ion.

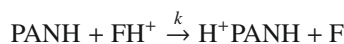
Protonated PANHs (H⁺PANH) were produced by chemical ionization (CI) reactions (Munson & Field 1966) occurring in the trap after formation of the radical cation PANH (and its fragments) by UV-photoionization. These reactions can be controlled by pressure P in the ion source and the extraction time delay (trapping time). Self-chemical ionization (McLuckey et al. 1988) is likely to be responsible for the generation of most of the protonated PANHs studied here



where the second product on the righthand side is the radical neutral PANH after losing an H atom. As an example, consider the formation of protonated phenanthridine (H⁺phenanthridine) in Fig. 1. The measured rate of formation of H⁺phenanthridine at a fixed pressure of 7×10^{-5} mbar is depicted in the inset. The figure also shows the ion peaks for radical (m/z 179) and protonated (m/z 180) phenanthridine cations, and the ion fragments produced when both ionic forms were irradiated with FELIX at $9.5 \mu\text{m}$. The ion signal of H⁺phenanthridine (squares) as a function of time delay behaves according to typical first-order kinetics: $1 - \exp(-kt)$.

For the acridine molecule, it was observed that, even at high pressures ($\sim 1 \times 10^{-4}$ mbar), the rate constant associated with the

formation of H⁺acridine was not as high as for the other species, and a complementary process was used to facilitate the generation of a strong protonated signal, i.e.,



where FH⁺ is a UV induced fragment ion. A time delay between the UV laser and the RF amplitude pulse used for mass isolation is introduced to allow more time for FH⁺ to protonate the neutral PANH species. Since the proton affinity (PA) of the PANH is likely higher than the PA of any fragment F not containing an N-atom, the process is exothermic and protonation of the PANH occurs.

2.2. Theoretical

PANH ion structures in radical (PANH⁺) and protonated (H⁺PANH) forms are optimized followed by calculation of their harmonic frequencies and IR intensities using the 3-parameter hybrid density functional theory (DFT) method B3LYP (Becke 1993) with a triple- ζ basis set (6-311G(d,p)). For some structures, the B3PW91 and BP86 methods are also employed. Theoretical spectra are generated by convoluting the DFT frequencies and intensities with a Gaussian lineshape function of 30 cm^{-1} FWHM. Although it is expected that each experimental IRMPD band possesses a linewidth that varies with the vibrational mode, the FWHM value used gives a reasonable broadening that compares well with the linewidth of most measured IRMPD bands of the different PANH structures.

The anharmonicity of the measured IRMPD bands are taken into account by scaling the DFT frequencies by a factor of 0.9679 (Andersson & Uvdal 2005). DFT calculations are carried out using Gaussian 03 (Frisch 2004).

3. Results and discussion

3.1. IRMPD spectra of ionized PANH species

3.1.1. Quinoline

The quinoline molecule is an N-substituted version of naphthalene (C₁₀H₈). The gas phase IRMPD spectra of ionized quinoline in radical (m/z 129) and protonated (m/z 130) forms retrieved at approximately 5×10^{-6} and 1×10^{-5} mbar, respectively, are shown in Fig. 2. After resonant irradiation with FELIX, a rich fragmentation pattern was observed for both ionic forms. The major IRMPD fragments were observed at m/z 103, m/z 77 (probably phenyl cation, C₆H₅⁺), m/z 65 (probably C₅H₅⁺) for quinoline⁺, and m/z 103 and m/z 77 for H⁺quinoline. Identifying the fragment ion structures is unimportant for obtaining the IRMPD spectra of the parent ion.

The IRMPD spectrum of H⁺quinoline (Fig. 2) is unambiguously recognized by the strong band centered at 772 cm^{-1} owing to the strong CH out-of-plane bending mode. This band is observed just 4 cm^{-1} redshifted from its calculated position at 776 cm^{-1} ($12.8 \mu\text{m}$), and is three times more intense than its counterpart CH out-of-plane band in quinoline⁺ (Fig. 2) as indicated by the theoretical spectra. Conversely, the intensities of the H⁺quinoline CH and CC inplane modes in the $1100\text{--}1600 \text{ cm}^{-1}$ region decrease to nearly half the values observed in the radical PANH cation, which agrees with the calculations.

The frequencies of the CH out-of-plane vibrations are mainly determined by the number of adjacent CH units on the periphery of an aromatic ring (Hudgins & Allamandola 1999b). The H⁺quinoline 772 cm^{-1} feature is clearly caused by a pair of

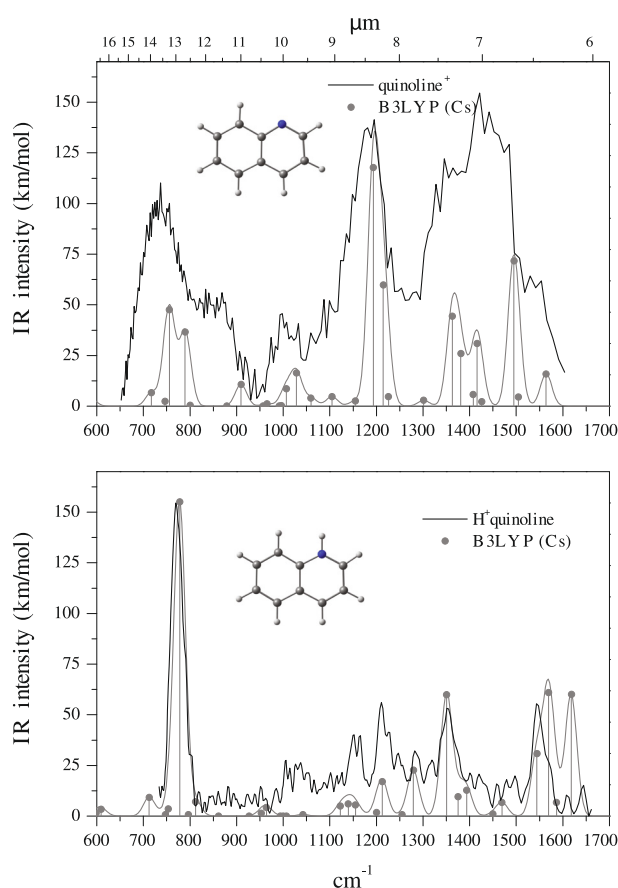


Fig. 2. IRMPD spectra of radical and protonated quinoline cations (*top and bottom panels*, respectively) compared to their corresponding DFT calculated spectra at the B3LYP/6–311G(d, p) level.

four adjacent CH units (two groups of the quartet class). For quinoline⁺, there are two partially resolved bands with peak positions that correlate with the two CH adjacency classes present in quinoline. The band calculated at 756 cm⁻¹ (13.2 μm) is due to the CH-quartet, and the slightly less intense band at 787 cm⁻¹ (12.7 μm) comes from three adjacent CH units (one CH-trio class). These two bands appear to be strongly broadened by the multiple-photon excitation process (Oomens et al. 2006, 2003, 2000), and are observed at 738 and 842 cm⁻¹. The difference in strength of CH out-of-plane H⁺quinoline and quinoline⁺ features is a consequence of the oscillator strength carried by a single CH-quartet mode in the protonated structure, while for the radical, it is split into two different nearby modes of A'' symmetry, which are therefore likely coupled and possibly share some intensity.

According to the DFT calculation, the strongest quinoline⁺ spectral feature is a CH inplane bending band at 1197 cm⁻¹ (8.35 μm), which appears slightly redshifted in the IRMPD spectrum at 1185 cm⁻¹. The observed intensity of this band is comparable to the intensity of the other prominent bands, while it is predicted to be twice as intense as the next intense band (located to the blue). While the reason for this discrepancy is unknown, we note that the intensities in an IRMPD spectrum may be influenced by nonlinear effects in the multiple-photon excitation process and that computed intensities may not be as accurate as, for example, the computed frequencies of the vibrational modes. In addition, this intense band appears much weaker in the H⁺quinoline spectrum.

To the high-frequency end of the quinoline⁺ IRMPD spectrum, there are three unresolved bands with mixed CH inplane/CC stretching mode character at 1370, 1450, and 1540 cm⁻¹. The redshift of these bands is on average 1.6% compared to their theoretical values. This suggests that the effects of anharmonicity are more pronounced when CC modes are involved, in accordance with the IRMPD spectra of the counterpart PAH cations (Oomens et al. 2003). For the H⁺quinoline spectrum, the three next most prominent features are predicted at 1350 cm⁻¹ (mixed CH inplane/CC stretching) and at 1564 and 1618 cm⁻¹ (both CC stretching). The first two bands appear resolved in the IRMPD spectrum at 1354 and 1548 cm⁻¹. Somewhat to our surprise, the strongest band near the 6.2 μm region at 1618 cm⁻¹ is not clearly observed. Nonetheless, the IRMPD spectra show that the CC-stretching vibrations in H⁺quinoline appear at higher frequencies than in quinoline⁺.

3.1.2. Isoquinoline

This molecule is an isomer of quinoline, and upon ionization, the radical cation structure isoquinoline⁺ is 0.028 eV (ZPE-corrected B3LYP/6–311G(d, p) calculation) more stable than its counterpart quinoline⁺. IRMPD experiments for isoquinoline were performed under conditions that are qualitatively similar to quinoline. Again, multiple fragmentation channels are observed for both ionic forms of isoquinoline, which typically occurs when ions are excited to internal energies well above their dissociation thresholds (Dunbar et al. 2006). The observed IRMPD cationic fragments are *m/z* 103, *m/z* 89, and *m/z* 76 for isoquinoline⁺, and *m/z* 103 for H⁺isoquinoline. A subtle difference compared to quinoline is the absence of the lowest mass fragments (*m/z* 77 in H⁺quinoline, and 65 in quinoline⁺), which is possibly due to the higher stability of isoquinoline in the radical cation form.

Figure 3 shows the measured IRMPD spectra retrieved via the ionic fragments at *m/z* 102 and *m/z* 103, at pressures of $\sim 1 \times 10^{-6}$ and 6×10^{-5} mbar, for isoquinoline⁺ and H⁺isoquinoline, respectively. Both isoquinoline⁺ and H⁺isoquinoline IR spectra are predicted to be qualitatively similar to their counterpart quinoline cationic forms. Subtle differences, especially for the radical forms, are seen around 750 and 1400 cm⁻¹ (compare with Fig. 2).

The differences are understood by considering whether nitrogen substitution takes place on the α (quinoline) or β (isoquinoline) carbon positions. For the radical cation, when the N-atom is in the β position (isoquinoline⁺), the induced charge effects are diluted into the same ring and have almost no influence on the other one, whereas for α -position N-substitution (quinoline⁺), the charge effects reach the other ring, and IR activities are more delocalized among modes. These effects are seen in the IRMPD spectrum of quinoline⁺ as two broad absorption features in the 700–800 and 1300–1600 cm⁻¹ ranges due to CH out-of-plane and mixed CH inplane/CC stretch modes, respectively. For isoquinoline⁺, on the other hand, the IRMPD spectrum more closely resembles that of the parent PAH⁺ naphthalene (vide infra).

For the protonated species, the position of the N-atom does not have a noticeable influence on the out-of-plane CH features, as seen in the IRMPD and DFT spectra of H⁺isoquinoline and H⁺quinoline. Conversely, there are predicted differences in CH inplane and CC stretch modes, but because of the missing 1618 cm⁻¹ band in the IRMPD spectrum of quinoline⁺, this could not be experimentally verified. Unlike for quinoline⁺, the strongest CC stretch band near 6.2 μm for H⁺isoquinoline,

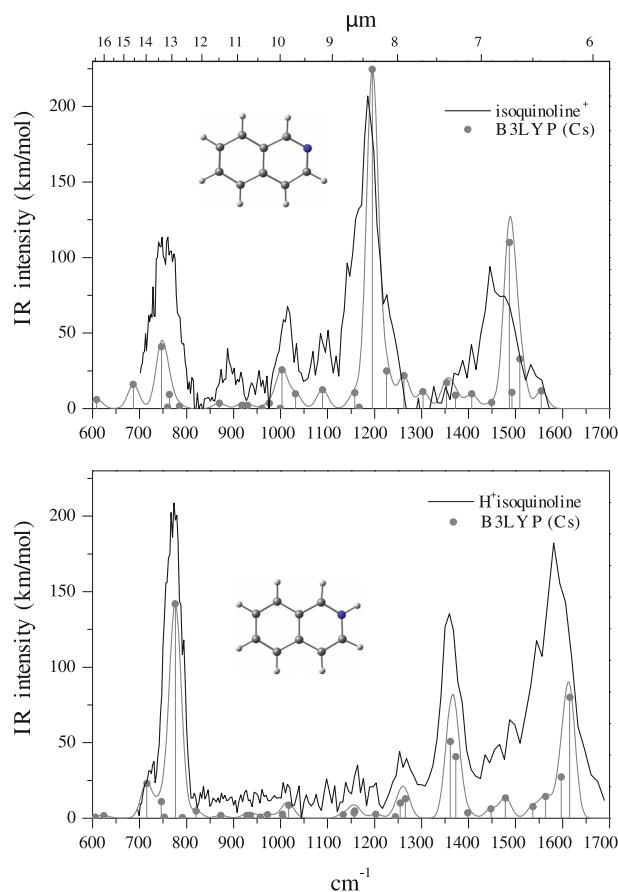


Fig. 3. IRMPD spectra of radical and protonated isoquinoline cations (top and bottom panels, respectively) compared to their corresponding DFT calculated spectra at the B3LYP/6–311G(d, p) level.

predicted at 1611 cm^{-1} ($6.21\text{ }\mu\text{m}$), appears in the IRMPD spectrum at 1582 cm^{-1} ($6.32\text{ }\mu\text{m}$) and carries CN stretch and NH inplane bending character.

Similar differences between radical cation and protonated IRMPD spectra are observed for quinoline and isoquinoline. The CH out-of-plane bending modes appear sharper and more intense in the protonated species than in the radical cations. The intense CH inplane band observed around 1200 cm^{-1} for the radical cations appears much weaker and/or shifted toward higher frequencies in the protonated species. Finally, the CC-stretching modes are observed at higher frequencies for the protonated species than the radical cations.

3.1.3. Benzo[h]quinoline

The benzo[h]quinoline molecule has a phenanthrene skeleton with the N-atom substituted on the inner side of one of the equivalent outer rings. Because of its low vapor pressure, the graphite oven was used for evaporation at an approximate temperature of $37\text{ }^{\circ}\text{C}$. Upon IR multiple-photon excitation at $9\text{ }\mu\text{m}$, the radical cation ($m/z\ 179$) dissociates into $m/z\ 153$ and $m/z\ 126$ fragments.

Figure 4 shows the IRMPD spectrum of benzo[h]quinoline⁺ recorded by monitoring these fragments. In the longer wavelength region, the calculated DFT spectrum shows three CH out-of-plane bending modes with peak positions at 687 , 749 and 848 cm^{-1} . The former band is caused by a CH-duo group (two adjacent CH-units on one ring), and is the only one to have a well localized origin. These three A'' symmetry bands

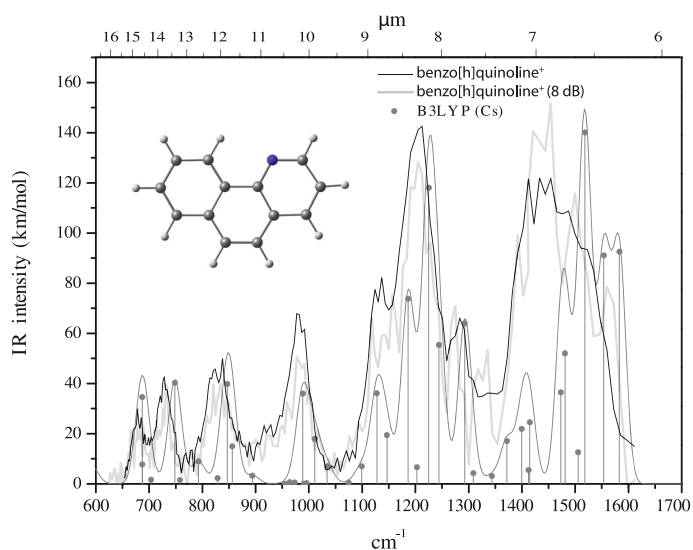


Fig. 4. IRMPD spectrum of benzo[h]quinoline radical cation recorded with the unattenuated (black) and 8 dB attenuated (light gray) FELIX beam, and DFT calculated spectrum at the B3LYP/6–311G(d, p) level.

are resolved in the IRMPD spectrum at 680 , 728 , and 828 cm^{-1} , thus redshifted compared to theory by 1, 2.8, and 2.4%, respectively. The IRMPD band observed at 980 cm^{-1} is redshifted by 1.2%, and according to theory, this feature is dominated by a CNC inplane bending mode, which falls slightly below the low-frequency limit ($<1000\text{ cm}^{-1}$) where these modes were noticed for four-ring PANH cationic structures (Mattiola et al. 2003). While this band is predicted to be of comparable intensity to the three CH out-of-plane bands, it is more intense by $\sim 30\%$ in the experiment.

Next, in the $1100\text{--}1300\text{ cm}^{-1}$ range, three partially resolved CH inplane IRMPD bands are observed at 1130 , 1202 , and 1279 cm^{-1} . While the 1130 and 1279 cm^{-1} bands have peak positions in reasonable agreement with the DFT spectrum (redshifted by 0.26 and 1.1% respectively), the 1202 cm^{-1} IRMPD band is found 2.2% more to the red than predicted (1229 cm^{-1}), which is due to overlapping of the 1229 cm^{-1} band with a medium-intensity band calculated at 1186 cm^{-1} . The average peak position of both bands is then 1207 cm^{-1} , which corrects the redshift of the IRMPD band to about 0.4%. Besides the 980 cm^{-1} feature, the 1279 cm^{-1} IRMPD band also carries a strong CN stretching character.

Finally, an unresolved feature of almost 110 cm^{-1} FWHM is observed in the $1350\text{--}1600\text{ cm}^{-1}$ spectral region. According to the DFT calculation, this region is dominated by closely-spaced delocalized CC stretching and CH inplane bending modes. Although the lack of resolved peaks does not permit judging the amount of redshift in individual bands, the whole feature is estimated to be redshifted by at least 4%. The high redshift points towards a relatively high anharmonicity for these modes, which may also explain the lack of resolved spectral structure, as higher anharmonicities usually result in more extensive broadening of bands as well (Oomens et al. 2006, 2004, 2003). Figure 4 also shows the IRMPD spectrum recorded with the IR intensity attenuated by 8 dB. This spectrum represents a single FELIX scan, hence the lower signal-to-noise ratio. As a result of the lower laser fluence, more spectral details become evident, particularly for the band predicted at 1407 cm^{-1} , which is clearly masked in the higher fluence IRMPD spectrum. Furthermore,

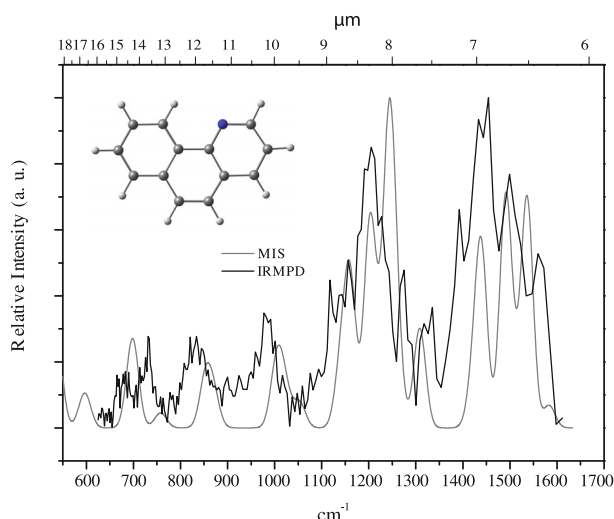


Fig. 5. Comparison of IR spectra of benzo[h]quinoline radical cation recorded via argon matrix-isolation spectroscopy (Mattioda et al. 2003) (MIS) and IRMPD techniques.

the four partly resolved IRMPD bands in the 1450–1600 cm^{-1} range compare fairly well to the DFT spectrum.

In Fig. 5, we compare our benzo[h]quinoline⁺ IRMPD spectrum (recorded with 8 dB attenuation of the IR beam) with the spectrum recorded using argon matrix-isolation spectroscopy (MIS) by Mattioda et al. (2003). The MIS intensities are convoluted with a 30 cm^{-1} FWHM Gaussian lineshape function for better visual inspection. A first distinction is found in the out-of-plane CH bending bands. In the 8 dB attenuated IRMPD spectrum (Fig. 4), these bands are located at 680, 729, 834, and 983 cm^{-1} , while in the MIS spectrum the positions are blueshifted to 698, 757, 858 and 1003 cm^{-1} , respectively. In the high-energy region of the spectrum, a roughly similar redshift of the bands in the IRMPD spectrum is observed compared to those in the MIS spectrum. Although caused by the higher spectral congestion here, it is more difficult to establish the correct correlation between the bands in the two spectra. The nonlinear absorption nature of multiple-photon absorption in IRMPD is known to induce a redshift as a consequence of vibrational anharmonicity (Oomens et al. 2003). In addition, the higher temperature of the benzo[h]quinoline cations in our experiment as compared to the temperature in the MIS technique may induce another redshift (Joblin et al. 1995). The interstellar emission spectrum is very likely also redshifted from a 0-K spectrum owing to vibrational anharmonicity (Barker et al. 1987; Cook & Saykally 1998).

3.1.4. Phenanthridine

The phenanthridine molecule is an isomer of benzo[h]quinoline with the N-atom replacing one of the CH units of the central aromatic ring. The IRMPD spectrum of the radical cation (phenanthridine⁺) was recorded by monitoring the fragment peak at m/z 152.

Figure 6 (top panel) shows the IRMPD spectrum along with theoretical spectra generated by B3LYP and BP86 DFT methods. Using BP86 reduces the C_s symmetry of the planar phenanthridine⁺ structure to a nonplanar C_1 structure. In the entire 600–1600 cm^{-1} region deviation from both DFT methods is evident becoming more severe for the B3LYP spectrum. Especially the intensity of the 738 cm^{-1} IRMPD band is strongly

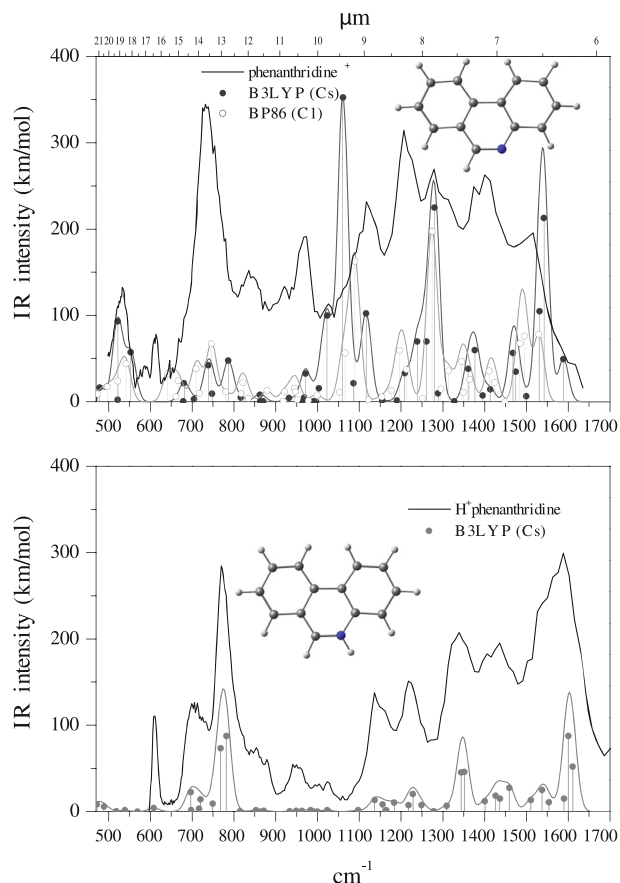


Fig. 6. IRMPD spectra of radical and protonated phenanthridine cations (top and bottom panels, respectively) compared to their corresponding DFT spectra (B3LYP/6–311G(d, p)). The top panel also shows the spectrum calculated with the BP86 method.

mis-calculated by both methods. In the case of B3LYP, increasing the basis set from 6–311G(d, p) to 6–311G(2d, 2p), optimizing at the C_1 symmetry or adding diffuse functions (6–311++G(d, p)) yield the same spectra. Using the B3PW91 method with the 6–311G(d, p) basis set generates essentially the same spectrum as B3LYP. Despite the large disagreement in peak positions, in particular in the 1100–1600 cm^{-1} region, the BP86 approach seems to give a similar trend in relative intensities for the 1123, 1213, and 1397 cm^{-1} IRMPD bands, predicted at 1089, 1274 and 1490 cm^{-1} , respectively. The ability of the BP86 method to reproduce the experimental spectra in some cases better than the B3LYP method was noticed before in a computational study of five-membered ring PAHs (Bauschlicher et al. 1999). The IRMPD spectrum was also recorded in the 500–600 cm^{-1} region, although all DFT methods predict the medium intensity band owing to a skeletal breathing mode in accordance with the IRMPD band observed at 530 cm^{-1} .

The failure of the computational methods to reproduce the experimental spectrum of phenanthridine⁺ thus remains somewhat mysterious, especially since these methods perform so well for the other PANH⁺s in this study and since no matrix-isolation spectrum was reported for this species in the study of Mattioda et al. (2003). Perhaps, the disagreement with theory is due to a low-lying electronic state not accounted for by the DFT calculations, as has also been suggested for the parent PAH cation of phenanthrene (Piest et al. 2001).

The formation of protonated phenanthridine (H⁺phenanthridine) was reviewed in the experimental section. In Fig. 1 it

is seen that resonant irradiation with FELIX results in a fragmentation pattern similar to phenanthridine⁺, but the major peak is at m/z 153 and not m/z 152. The bottom panel of Fig. 6 shows the IRMPD spectrum of H⁺phenanthridine acquired via the m/z 153 fragment. Overall, it is observed that experimental and calculated (B3LYP) spectra agree fairly well, although the IRMPD bands in the 1100–1600 cm⁻¹ region are only partially resolved. Similar to benzo[h]quinoline⁺ or phenanthridine⁺, this region contains many closely-spaced CH inplane/CC stretching modes, which are subject to anharmonic broadening effects. This is exemplified by comparing the two regions 700–800 and 1500–1650 cm⁻¹, where the same band structure is predicted, a strong absorption accompanied by a shoulder to the red. It is noticed that the CH out-of-plane bands at 701 and 774 cm⁻¹ are resolved in the IRMPD spectrum at 711 and 774 cm⁻¹, respectively, while in the high-frequency region, the predicted CC stretch bands at 1541 and 1603 cm⁻¹ appear as an unresolved IRMPD band with a central peak position estimated at 1582 cm⁻¹.

Another slight deviation from theory is the three barely unnoticeable bands at 608, 858, and 980 cm⁻¹, which in the IRMPD spectrum appear at 611, 869 and 951 cm⁻¹ with substantial intensity. Interestingly, the three bands have the same ring-deformation mode character.

3.1.5. Acridine

The acridine molecule has the PAH framework of anthracene with the N-atom substituted in the central aromatic ring. The IRMPD spectrum of the radical cation form (acridine⁺), shown in the top panel in Fig. 7 along with the DFT calculated spectrum, was obtained by summing the spectral response of the two observed IRMPD fragments at m/z 151 and 126. The ion trap pressure during the experiment was $\sim 3 \times 10^{-6}$ mbar.

Comparison with the calculated DFT spectrum reveals an enhanced experimental intensity of all absorption bands relative to the two strongest features at 1217 and 1305 cm⁻¹. Particularly, the weak inplane CH bending absorption shoulder predicted at 1150 cm⁻¹ is observed to be much stronger in the IRMPD spectrum, where it appears as a partially resolved narrow band of medium intensity at 1154 cm⁻¹. Another CH inplane bending mode with almost no calculated intensity (1.57 km mol⁻¹) predicted at 1080 cm⁻¹ is clearly observed as a weak fairly well-resolved band at 1085 cm⁻¹. Toward the high-frequency end, in the 1400–1600 cm⁻¹ range, three semi-resolved IRMPD bands of mixed CH inplane bending and CC stretching character are observed at 1462, 1517, and 1572 cm⁻¹. The most intense band at 1305 cm⁻¹ is the only mode exhibiting a strong CN stretching character.

The intensity enhancement of IR absorptions was also seen for quinoline⁺. It is possibly caused by saturation effects on the strongest bands. While the overall dissociation yield is only a few percent, the overlap of the IR beam with the ion cloud is not well known, so that it is possible that virtually all ions that overlap with the laser beam are dissociated. This effect would artificially enhance the intensity of the weaker modes in the spectrum relative to the stronger ones.

The IRMPD spectrum of protonated acridine (H⁺acridine) recorded at the HCN-loss dissociation channel at a pressure of 1×10^{-4} mbar is shown in the bottom panel of Fig. 7. The expected strong CH out-of-plane band calculated at 764 cm⁻¹ appears in the IRMPD spectrum at 756 cm⁻¹. The redshift is thus 1% and is typical of bands with CH out-of-plane character. Moreover, the predicted absorption at 1614 cm⁻¹ due to

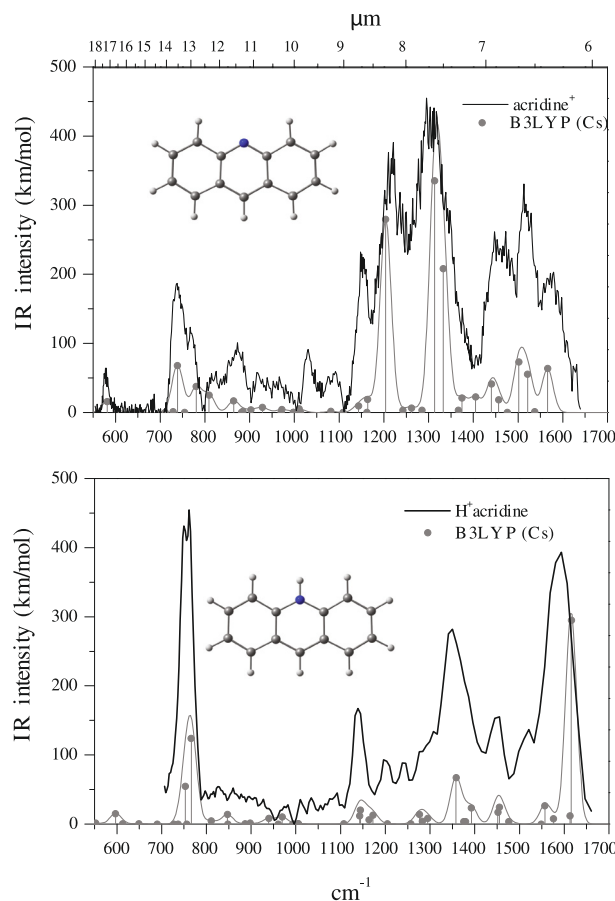


Fig. 7. IRMPD spectra of radical and protonated acridine cations compared to their corresponding DFT spectra (B3LYP/6-311Gdp) in the top and bottom panels, respectively.

CC skeletal vibration with a strong NH inplane character contribution is observed at 1587 cm⁻¹. This band exhibits a redshift of 1.7%, which is typical of modes in this frequency range, see e.g. H⁺phenanthridine, H⁺isoquinoline, or radical cation PAH species (Oomens et al. 2003, 2000). The lower laser power toward wavelengths of 6 μ m likely explains the lower relative intensity of the 1587 cm⁻¹ band.

In comparison, the spectral characteristics for acridine⁺ and H⁺acridine are grossly similar to those of the other PANHs studied here: a stronger CH out-of-plane mode for the protonated species, much stronger CH inplane modes in the radical cation, and a blueshifted CC stretch mode in the protonated species compared to the radical cation.

3.1.6. Dibenzof[h]quinoline

The dibenzof[h]quinoline molecule is an N-substituted version of triphenylene, and its structure resembles that of benzo[h]quinoline with an extra ring fused to the middle one. For this species, only the spectrum of the radical cation was recorded, monitoring the HCN-loss channel.

Figure 8 shows a comparison of the IRMPD spectrum of dibenzof[h]quinoline⁺ and the B3LYP theoretical spectrum, and in addition the spectrum calculated using the BP86 functional. Similar to phenanthridine⁺, the absorption bands due to CH inplane bending and CC stretching modes present a large anharmonic shift ($\sim 5\%$) compared to the band positions calculated by the B3LYP functional. On the other hand, a better overall match

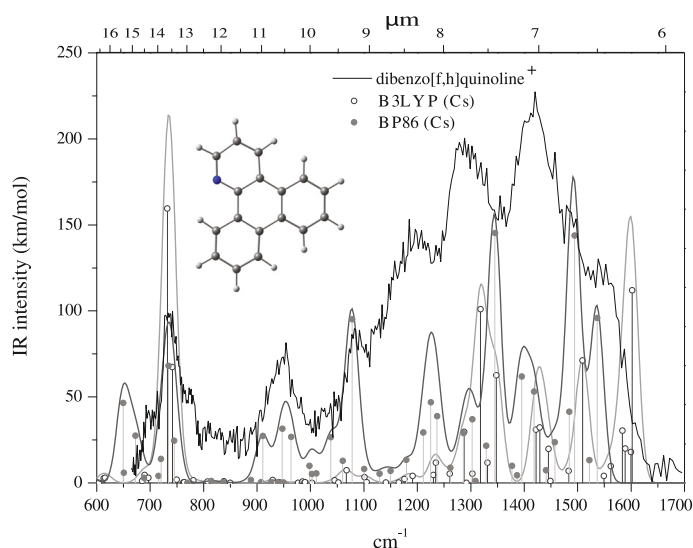


Fig. 8. IRMPD spectrum of dibenzo[f,h]quinoline radical cation and DFT spectra calculated with B3LYP and BP86 methods using the 6–311G(d, p) basis set.

is observed between IRMPD and BP86 calculated spectra of dibenzo[f,h]quinoline⁺, both in terms of peak positions and relative intensities. Unlike for phenanthridine⁺, the BP86 method retains the planarity for dibenzo[f,h]quinoline⁺. Both B3LYP and BP86 spectra show a congested mid-IR region with numerous IR-active modes, whereas the CH out-of-plane modes appear as reasonably well-resolved bands in the IRMPD spectrum (bands at 738 cm⁻¹, due to two CH-quartets, and at 947 cm⁻¹). A broad feature extends from 1050 to 1600 cm⁻¹, where bands are not resolved individually. The most prominent partially resolved band at 1418 cm⁻¹ presents a redshift of ~5% and 7.7% as compared to the BP86 and B3LYP calculated bands, respectively. Similar disagreements between DFT-computed and IRMPD spectra have been found previously for the triphenylene cation, although there it was suggested that they are caused by Jahn-Teller distortion (Oomens et al. 2003), which does not occur in the N-substituted ion.

3.2. PANH ion (+, H⁺) spectra and their relevance to the astrophysical UIR emissions

Except for the CH stretch modes near 3.3 μm, the IR intensities of non-nitrogenated PAHs increase substantially upon ionization (Pauzat et al. 1992; Allamandola et al. 1999), where the CC and CH inplane modes are significantly more enhanced than the CH out-of-plane modes. Similar ionization effects are observed here for gas-phase PANHs as in the argon matrix-isolated spectra of Mattioda et al. (2003). In the present work an interesting exception was found for phenanthridine⁺, where the experimental intensity of the out-of-plane CH band (738 cm⁻¹) is of comparable intensity to the CC-stretching bands in the 1100–1600 cm⁻¹ region. The strong CH out-of-plane band at 742 cm⁻¹ in the IR spectrum of neutral phenanthridine (see NIST Chemistry Webbook) compares reasonably well with the phenanthridine⁺ 738 cm⁻¹ band.

Substituting an N-atom into the aromatic framework of PAHs has the significant effect of reducing their symmetry. The atomic displacements along a normal coordinate that leave the electric dipole moment unchanged in the PAH do produce such a change in the corresponding PANH, and this normal mode

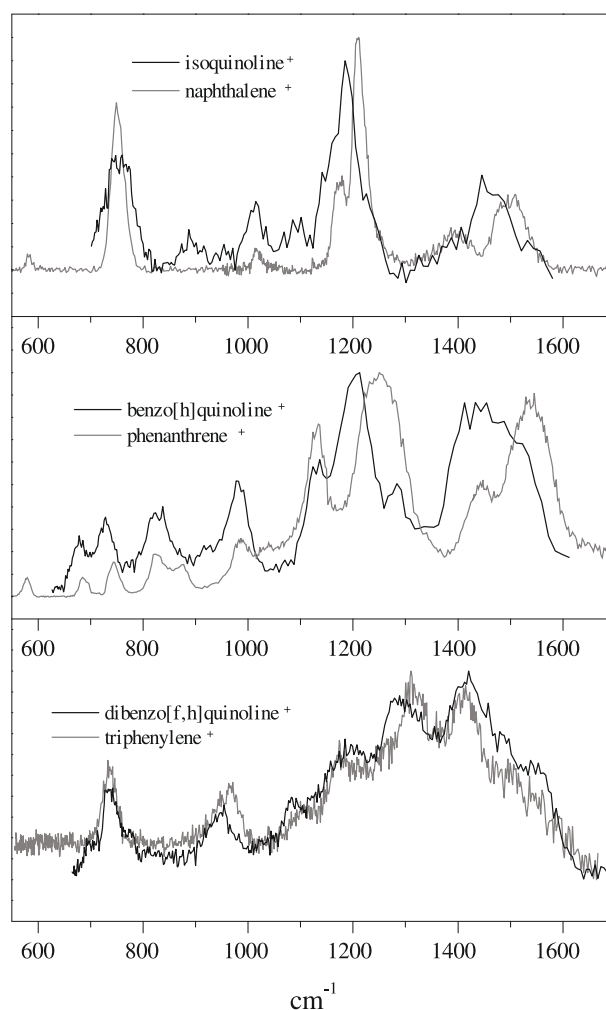


Fig. 9. Comparison of experimental IR spectra of PAH⁺ and PANH⁺ species.

becomes IR-active. Although the experimental IRMPD spectra of PANH⁺ species indeed show broader bands as a result, the overall effect observed on the mid-IR spectra is mild and it is not expected to make a substantial difference in terms of the UIR emission bands. For instance in Fig. 9, the four-ring PANH radical cation dibenzo[f,h]quinoline⁺ is almost indistinguishable from its PAH parent cation triphenylene (taken from Oomens et al. 2006). The same figure shows the two-ring species isoquinoline⁺ and cationic naphthalene, where PANH⁺ and PAH⁺ mid-IR spectra are alike, although bands of the PANH⁺ are broader. Here, one notices that the strongest isoquinoline⁺ CC stretching band near the 6.2 μm region is actually redshifted with respect to the analogous band in naphthalene⁺. This is also clearly observed for benzo[h]quinoline⁺ and its parent PAH phenanthrene. Based on a matrix isolation spectroscopy study of several small PANHs (Mattioda et al. 2003), Hudgins et al. (2005) observed that the strongest CC stretching band tends to shift toward longer wavelengths in accordance with our observations.

These considerations indicate that the CC stretching vibrations of small gas-phase PANH radical cations cannot account for the interstellar 6.2 μm UIR band. Nonetheless, because of the similarity to IR spectra of PAH⁺ species, their contribution to the remaining UIR bands cannot be dismissed. This confirms the conclusions of a computational study on PANH cations

Table 2. Calculated and experimental (in parentheses) positions of the strongest band in the 6.2 μm region for the PANH ions studied here (in cm^{-1}).

PANH	+	H ⁺
Quinoline	1563 (1541)	1618 (1548 ¹)
Isoquinoline	1556 (1543)	1611 (1582)
Phenanthridine	1490 ² (1508)	1603 (1582)
Benzo[h]quinoline	1579 (1557)	1590 (1578 ³)
Acridine	1565 (1572)	1614 (1587)
1-azapyrene	1518 (1549 ⁴)	1592 (1597 ⁵)
Dibenzo[f,h]quinoline	1582(1544)	1599 (...)

Notes. ⁽¹⁾ Corresponds to the highest-frequency band seen in the H⁺quinoline IRMPD spectrum predicted at 1564 cm^{-1} . ⁽²⁾ Value calculated using the BP86 DFT method. ⁽³⁾ M. T. Vala, personal communication. ⁽⁴⁾ Band corresponds to isomer 2-azapyrene, for which the strongest band in the 6.2 μm region is predicted at 1526 cm^{-1} , shifted by 8 cm^{-1} from the band in 1-azapyrene (Mattioda et al. 2003). ⁽⁵⁾ Vala et al. (2009a).

(Bauschlicher 1998; Langhoff et al. 1998), as well as those of the MIS study (Hudgins et al. 2005; Mattioda et al. 2003).

In their protonated form (H⁺PANH), however, the N-substituted PAHs present a significantly different IR spectrum, which is reflected in both peak positions and band intensities. The CH out-of-plane modes are observed as the strongest bands in the spectrum, similar to these bands in neutral PANHs, and the CC-stretching modes show an enhancement in intensity similar to what is observed for cationic PANH species. For instance, the CH out-of-plane H⁺PANH features in the 700–800 cm^{-1} region are at least twice as intense as the PANH⁺ features. The strong CH inplane PANH⁺ modes, usually accompanied by N-atom displacement, decrease in strength in H⁺PANH species. The H⁺PANH CC modes slightly increase in strength and their frequencies shift to the blue with respect to PANH⁺ CC modes. As a result, when comparing the position of the strongest CC-stretching band in the 6.2 μm region of H⁺PANH and PANH⁺ species, a systematic blueshift of the H⁺PANH bands is observed. This is summarized in Table 2 where calculated and experimental peak positions of the strongest CC stretching bands are listed for all PANHs investigated. The four-ring pericondensed PANH 1-azapyrene is also included, and the experimental band positions of radical and protonated forms are obtained from Mattioda et al. (2003) and Vala et al. (2009a), respectively.

Although experimental IRMPD bands are generally observed at lower frequencies than predicted, the blueshift of the bands in the 6.2 μm region in H⁺PANHs relative to PANH⁺s is evident. In a recent study of the IRMPD spectra of protonated PAH species (H⁺PAH), it is also observed that the H⁺PAH CC bands in the 6.2 μm region appear at higher frequencies than the analogous bands in the radical cation PAH⁺ species (Knorke et al. 2009). In addition, the H⁺PANH bands appear slightly farther to the blue than the H⁺PAH bands; for protonated anthracene, the IRMPD feature is observed at 1575 cm^{-1} (Knorke et al. 2009), whereas in its corresponding H⁺PANH form (acridine), the IRMPD feature is observed at 1587 cm^{-1} . Protonation of anthracene occurs at the same position where the N-atom is substituted in acridine.

We now consider the astrophysically more relevant PAH coronene. While no experimental data are available for N-substituted coronene, we compared calculated band positions for the four forms PAH⁺, H⁺PAH, PANH⁺, and H⁺PANH. The

Table 3. Position (in cm^{-1}) of the strongest band in the 6.2 μm region for coronene.

Form	Calc ¹ (Exp)
PAH ⁺	1555 (1533)
H ⁺ PAH	1591 (1588)
PANH ⁺	1548 (...)
H ⁺ PANH	1597 (...)

Notes. ⁽¹⁾ Frequencies calculated at the B3LYP/6–311G(d, p) level and scaled by 0.9679.

calculated peak positions for the dominant CC stretch band near 6.2 μm are listed in Table 3. As anticipated, the protonated forms (H⁺PAH and H⁺PANH) have predicted values at higher frequencies than their radical cation counterparts. In addition, the value for the H⁺PANH is again slightly higher than for the H⁺PAH. Previously, a computational study on H⁺PAHs (Hudgins et al. 2001) has already recognized the effect of the closed shell electronic structure on CC-stretch modes close to the 6.2 μm region, but until recently there has been no experimental verification of this trend.

Indeed, the joint effect of charge state and closed-shell electronic configuration typical of protonated PANHs causes the CC-stretching vibrations (including some NH inplane bending character) to appear at higher frequencies than in their respective radical cation PANH⁺ species. An earlier computational study of large PANH ions reports CC-stretching modes appearing at frequencies higher than 1610 cm^{-1} when the N-atom is substituted inside the PANH skeleton (Hudgins et al. 2005), i.e., not on one of the CH units on the periphery of the molecule. Because of the endoskeletal N-substitution, these PANH cations have a closed-shell electronic structure, which explains the computed frequencies of the CC modes. Based on this, it has been pointed out that the CC stretch of large endoskeletal PANH cations can reproduce the observations of the 6.2 μm UIR emission (Hudgins et al. 2005). Our experimental spectra of protonated PANHs suggest that it is perhaps not so much the endoskeletal nature of the molecules that causes the higher frequency CC-stretch mode, but rather the closed-shell electronic structure, which the protonated peripheral PANHs and the cationic endoskeletal PANHs have in common.

The occurrence of protonated PANHs in interstellar environments is a plausible conjecture because of the high proton affinity of PANHs, the universal abundance of atomic hydrogen, and the presence of N-atom bearing molecules. If PANH molecules are present in astrophysical environments (Hudgins et al. 2005; Ricca et al. 2001), their protonated forms are certainly viable candidates as well.

Figure 10 shows the composite IR spectra (in equivalent proportions) obtained from the PANH structures measured in this work in comparison with the UIR bands from the source IRAS 23133+6050 (Sloan et al. 2003). The IR PANH⁺ spectrum in the middle panel corresponds to the four radical cationic PANH species quinoline⁺, isoquinoline⁺, benzo[h]quinoline⁺, and acridine⁺, and the one in the bottom panel to the four H⁺PANH species H⁺quinoline, H⁺isoquinoline, H⁺phenanthridine, and H⁺acridine. The astronomical source is an ultracompact H II region (Kurtz et al. 1999) sustained by an association of newborn massive stars. The predominantly UV radiation field emitted by these stars ionizes the material of the molecular cloud where the UIR emission originates.

As already stated above, the IR PANH⁺ bands deviate considerably from the UIR emissions. In particular, the 6.2 μm is

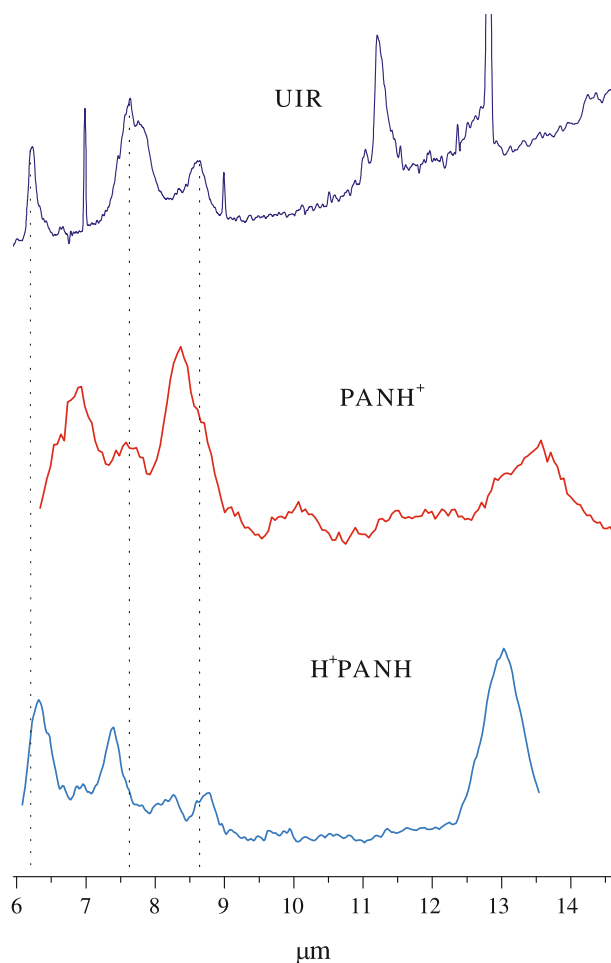


Fig. 10. Comparison of the UIR emission spectrum (*top panel*) characteristic of a molecular cloud (IRAS 23133+6050) with two composite IR gas-phase spectra of the radical cationic PANH species quinoline⁺, isoquinoline⁺, benzo[h]quinoline⁺, and acridine⁺ (*middle panel*) and of protonated PANH species H⁺quinoline, H⁺isoquinoline, H⁺phenanthridine, and H⁺acridine (*bottom panel*).

strongly redshifted with respect both the UIR and H⁺PANH analog bands. On the other hand, we noticed that the peak positions of two composite H⁺PANH IR absorption bands appear approximately 0.09 μm redshifted with respect the nominal 6.2 and 8.6 μm UIR emissions. This shift might be attributed to different degrees of anharmonic band shifting in the IRMPD experiments compared to the emission process giving rise to the interstellar bands. The spectral comparison in Fig. 10 shows a significant shift of the inplane hydrogen bending modes, which fall near 7.4 μm in the H⁺PANHs studied here, compared to the interstellar band at 7.7 μm. The shift of the inplane hydrogen bending mode is due to mode mixing of NH and CH bending vibrations. The band may redshift for larger PANHs, as also noted for regular PAHs (Hudgins & Allamandola 1999b). We also note that the nominal 7.7 μm interstellar band in fact consists of various subfeatures, which, depending on the source, include emission at 7.4 μm (Peeters et al. 2002). Finally, while interstellar emission spectra in the hydrogen stretching range show very few bands apart from the aromatic CH stretching bands around 3.3 μm, the calculated H⁺PANH spectra typically display a fairly intense band around 3.0 μm because of the NH-stretching mode. Interstellar PAH emission at this wavelength could, in some cases, be attenuated by ices in the cloud, which are known

to absorb strongly around 3.0 μm (Gibb et al. 2004). Moreover, further work will be required to verify the computed band position and relative intensity of these modes experimentally, especially since the bands in this region of the spectrum may be particularly sensitive to anharmonic effects (Barker et al. 1987; Cook & Saykally 1998).

4. Conclusions

Using the IR free-electron laser FELIX multiple-photon dissociation spectroscopy (IRMPD) was applied to measure the mid-IR spectra of ionized N-atom substituted polycyclic aromatic hydrocarbon (PANH) molecules in the gas phase. The observed IRMPD spectra were interpreted with theoretical spectra generated using DFT methods. With the exception of phenanthridine⁺, where none of the DFT approaches reproduced the experimental spectrum, an overall good agreement between measured IRMPD and calculated DFT bands was found.

Differences in the IR spectra of H⁺PANHs and PANH⁺s are observed in the 700–800 cm⁻¹ region, where the H⁺PANH out-of-plane CH features are at least twice as intense as in the radical cation PANH⁺ species. In the 6.2 μm region, the dominant CC-stretching band is shifted to higher frequencies in the protonated PANHs and intensities appear slightly enhanced. The CH inplane modes in the 1100–1300 cm⁻¹ region are significantly weaker in H⁺PANHs.

While the PANH⁺ species clearly cannot explain the 6.2 μm UIR emission, the remaining UIR bands are roughly reflected in the PANH⁺ spectra, which are quite similar to those of non-nitrogenated PAH⁺ species. On the other hand, the experimental IR spectra of the four H⁺PANH species investigated here appear to reproduce the 6.2 and 8.6 μm emissions rather closely, as is shown by comparison of their composite IR spectrum to a typical UIR emission spectrum (IRAS 23133+6050).

In conclusion, we have experimentally confirmed that nitrogen substitution in PAHs has significant consequences for their IR spectra, which are relevant to the UIR emission. Particularly the protonated form (H⁺PANH) of these species, with a closed-shell electronic structure, may contribute to the UIR spectrum. The effect of size and exact structure of the H⁺PANH species on their spectra remains to be investigated.

Acknowledgements. We would like to acknowledge Lex van der Meer, Britta Redlich, Giel Berden and other members of the FELIX staff for their skillful technical support. This work is part of the research program of FOM, which is financially supported by the Nederlandse Organisatie voor Wetenschappelijk Onderzoek (NWO).

References

- Allamandola, L. J., Hudgins, D. M., & Sandford, S. A. 1999, *ApJ*, 511, L115
- Andersson, M. P., & Uvdal, P. 2005, *J. Phys. Chem. A*, 109, 2937
- Baer, T., & Hase, W. L. 1996, *Unimolecular Reaction Dynamics* (Oxford University Press)
- Bagratashvili, V. N., Letokhov, V. S., Makarov, A. A., & Ryabov, E. A. 1985, *Multiple Photon Infrared Laser Photophysics and Photochemistry* (Harwood Academic Publishers)
- Barker, J., Allamandola, L., & Tielens, A. 1987, *ApJ*, 315, L61
- Bauschlicher, C. W. Jr. 1998, *Chem. Phys.*, 234, 87
- Bauschlicher, C. W. Jr., Hudgins, D. M., & Allamandola, L. J. 1999, *Theor. Chem. Acc.*, 103, 154
- Becke, A. D. 1993, *J. Chem. Phys.*, 98, 5648
- Beegle, L. W., Wdowiak, T. J., & Harrison, J. G. 2001, *Spectrochim. Acta A*, 57, 737
- Bernstein, M. P., Mattioda, A. L., Sandford, S. A., & Hudgins, D. M. 2005, *ApJ*, 626, 909
- Bregman, J. D., Hayward, T. L., & Sloan, G. C. 2000, *ApJ*, 544, L75
- Charnley, S. B., Kuan, Y.-J., Huang, H.-C., et al. 2005, *Adv. Space Res.*, 36, 137

- Cook, D., & Saykally, R. 1998, *ApJ*, 493, 793
- Dewar, M. J. S., & Worley, S. D. 1969, *J. Chem. Phys.*, 51, 263
- Dolgounitcheva, O., Zakrzewski, V. G., & Ortiz, J. V. 1997, *J. Phys. Chem. A*, 101, 8554
- Don McNaughton, P. D. Godfrey, R. D. B., & Thorwirth, S. 2007, *Phys. Chem. Chem. Phys.*, 9, 591
- Douberly, G. E., Ricks, A. M., v R. Schleyer, P., & Duncan, M. A. 2008, *J. Phys. Chem. A*, 112, 4869
- Dunbar, R. C., Moore, D. T., & Oomens, J. 2006, *J. Phys. Chem. A*, 110, 8316
- Elsila, J. E., Hammond, M. R., Bernstein, M. P., Sandford, S. A., & Zare, R. N. 2006, *Meteor. Planet. Sci.*, 41, 785
- Felker, P. M., & Zewail, A. H. 1985, *J. Chem. Phys.*, 82, 2975
- Frisch, M. J. 2004, Gaussian 03 (Gaussian, Inc., Wallingford CT)
- Gibb, E., Whittet, D., Boogert, A., & Tielens, A. 2004, *ApJS*, 151, 35
- Hony, S., Van Kerckhoven, C., Peeters, E., et al. 2001, *A&A*, 370, 1030
- Hudgins, D. M., & Allamandola, L. J. 1999a, *J. Phys. Chem. A*, 1089
- Hudgins, D. M., & Allamandola, L. J. 1999b, *ApJ*, 516, L41
- Hudgins, D. M., & Allamandola, L. J. 2002, *J. Phys. Chem.*, 99, 3033
- Hudgins, D. M., Bauschlicher, C. W., & Allamandola, L. J. 2001, *Spectrochim. Acta A*, 57, 907
- Hudgins, D. M., Bauschlicher Jr, C. W., & Allamandola, L. J. 2005, *ApJ*, 632, 316
- Joblin, C. 1998, in *Chemistry and Physics of Molecules and Grains in Space*, Faraday Discussions No. 109, 349
- Joblin, C., D'Hendecourt, L., Leger, A., & Defourneau, D. 1994, *A&A*, 281, 923
- Joblin, C., Boissel, P., Léger, A., d'Hendecourt, L., & Défourneau, D. 1995, *A&A*, 299, 835
- Kim, H. S., Wagner, D. R., & Saykally, R. J. 2001, *Phys. Rev. Lett.*, 86, 5691
- Knorke, H., Langer, J., Oomens, J., & Dopfer, O. 2009, *ApJ*, 706, L66
- Kurtz, S. E., Watson, A. M., Hofner, P., & Otte, B. 1999, *ApJ*, 514, 232
- Langhoff, S. R., Bauschlicher, C. W., Hudgins, D. M., Sandford, S. A., & Allamandola, L. J. 1998, *J. Phys. Chem. A*, 102, 1632
- Leger, A., & Puget, J. L. 1984, *A&A*, 137, L5
- Lehmann, K. K., Scoles, G., & Pate, B. H. 1994, *Ann. Rev. Phys. Chem.*, 45, 241
- Lorenz, U., Solca, N., Lemaire, J., Maitre, P., & Dopfer, O. 2007, *Angew. Chem. Int. Ed.*, 46, 6714
- Mattioda, A. L., Hudgins, D. M., Bauschlicher, C. W., Rosi, M., & Allamandola, L. J. 2003, *J. Phys. Chem. A*, 107, 1486
- Mattioda, A., Hudgins, D., Bauschlicher, C., & Allamandola, L. 2005, *Adv. Space. Res.*, 36, 156
- Mattioda, A. L., Rutter, L., Parkhill, J., et al. 2008, *ApJ*, 680, 1243
- McLucky, S. A., Glish, G. L., Asano, K. G., & Van Berkel, G. J. 1988, *Anal. Chem.*, 60, 2312
- McNaughton, D., Godfrey, P. D., Brown, R. D., Thorwirth, S., & Grabow, J.-U. 2008, *ApJ*, 678, 309
- Munson, M. S. B., & Field, F. H. 1966, *J. Am. Chem. Soc.*, 88, 2621
- Oepts, D., van der Meer, A. F. G., & van Amersfoort, P. W. 1995, *Infrared Phys. Technol.*, 36, 297
- Oomens, J., van Roij, A. J. A., Meijer, G., & von Helden, G. 2000, *ApJ*, 542, 404
- Oomens, J., Meijer, G., & von Helden, G. 2001, *J. Phys. Chem. A*, 105, 8302
- Oomens, J., von Helden, G., & Meijer, G. 2002, *Int. J. Mass Spectrom.*, 221, 163
- Oomens, J., Tielens, A. G. G. M., Sartakov, B. G., von Helden, G., & Meijer, G. 2003, *ApJ*, 591, 968
- Oomens, J., Moore, D. T., Meijer, G., & Helden, G. V. 2004, *Phys. Chem. Chem. Phys.*, 6, 710
- Oomens, J., Sartakov, B. G., Meijer, G., & von Helden, G. 2006, *Int. J. Mass Spectrom.*, 254, 1
- Paul, W. 1990, *Rev. Mod. Phys.*, 62, 531
- Pauzat, F., Talbi, D., Miller, M., DeFrees, D., & Ellinger, Y. 1992, *J. Phys. Chem.*, 96, 7882
- Peeters, E., Hony, S., Van Kerckhoven, C., et al. 2002, *A&A*, 390, 1089
- Peeters, Z., Botta, O., Charnley, S. B., et al. 2005, *A&A*, 433, 583
- Piest, H., von Helden, G., & Meijer, G. 1999, *ApJ*, 520, L75
- Piest, J. A. H., Oomens, J., Bakker, J., von Helden, G., & Meijer, G. 2001, *Spectrochim. Acta A*, 57, 717
- Pino, T., Dartois, E., Cao, A., et al. 2008, *A&A*, 490, 665
- Pirali, O., van-Oanh, N., Parneix, P., Vervloet, M., & Bréchnignac, P. 2006, *Phys. Chem. Chem. Phys.*, 8, 3707
- Ricca, A., Bauschlicher, C. W., & Rosi, M. 2001, *Chem. Phys. Lett.*, 347, 473
- Ricks, A. M., Douberly, G. E., & Duncan, M. A. 2009, *ApJ*, 702, 301
- Sephton 2002, *Nat. Prod. Rep.*, 19, 292
- Sloan, G. C., Hayward, T. L., Allamandola, L. J., et al. 1999, *ApJ*, 513, L65
- Sloan, G. C., Kraemer, K. E., Price, S. D., & Shipman, R. F. 2003, *ApJS*, 147, 379
- Szczepanski, J., & Vala, M. 1993a, *ApJ*, 414, 646
- Szczepanski, J., & Vala, M. 1993b, *Nature*, 363, 699
- Tielens, A. G. G. M. 2008, *ARA&A*, 46, 289
- Vala, M., Szczepanski, J., Dunbar, R., Oomens, J., & Steill, J. D. 2009a, *Chem. Phys. Lett.*, 473, 43
- Vala, M., Szczepanski, J., Oomens, J., & Steill, J. D. 2009b, *J. Am. Chem. Soc.*, 131, 5784